

CHEMISTRY

AN ASIAN JOURNAL

www.chemasianj.org

Accepted Article

Title: Synthesis and Characterization of Polycyclic Aromatic Hydrocarbons with Different Space-Constructions Based on the Hexaphenylbenzene Derivatives

Authors: Weizhi Wang, Hua Chen, Hao Yun Zhu, Yu Li Huang, and Jun Wei Yang

This manuscript has been accepted after peer review and appears as an Accepted Article online prior to editing, proofing, and formal publication of the final Version of Record (VoR). This work is currently citable by using the Digital Object Identifier (DOI) given below. The VoR will be published online in Early View as soon as possible and may be different to this Accepted Article as a result of editing. Readers should obtain the VoR from the journal website shown below when it is published to ensure accuracy of information. The authors are responsible for the content of this Accepted Article.

To be cited as: *Chem. Asian J.* 10.1002/asia.201701061

Link to VoR: <http://dx.doi.org/10.1002/asia.201701061>

A Journal of



A sister journal of *Angewandte Chemie* and *Chemistry – A European Journal*

WILEY-VCH

Synthesis and Characterization of Polycyclic Aromatic Hydrocarbons with Different Space-Constructions Based on the Hexaphenylbenzene Derivatives

Hua Chen, Haoyun Zhu, Yuli Huang, Junwei Yang, and Weizhi Wang*

Abstract: In recent years, low-bandgap polymers have attracted a wide range of attention in many fields. These compounds syntheses were focused on three factors according to the Roncali bandgap theory: 1) the degree of bond length alternation $E^{\delta r}$, 2) the aromatic resonance energy of the cycle E^{Res} , and 3) the substituted groups E^{Sub} . Now, we designed and prepared the low-bandgap polymers in a different way by the factor E^{θ} , the polymer chain deviation from planarity, and E^{Int} , the interaction of the molecular chains in the solid state. So, three polycyclic aromatic hydrocarbons with different space-constructions based on the hexaphenylbenzene derivatives were prepared in this work: linear type (P1-OX), V type (P2-OX) and zigzag type (P3-OX). These well-defined polymers exhibited the interesting behaviors in optics, electrochemistry due to their different extent of planarity. Matrix-assisted laser desorption ionization time-of-flight mass spectrometry (MALDI-TOF MS) gave the incremental orderly molecular weight distributions of P1, P2 and P3, whose weight-average molecular weights (\bar{M}_w) were 9000, 5500 and 69000, respectively. Their lamellar layer structures and π - π intermolecular stacking were demonstrated by two-dimensional grazing-incidence X-ray diffraction (2D-GIXRD), showing the edge-on chain conformation. At last, the materials were perfectly adopted to fabricate the high-performance organic field-effect transistor (OFET) devices, which revealed that these compounds would possess a great prospect as semiconductors.

Introduction

Conjugated polymers have attracted increasing attention in recent years due to their wide usages in various fields such as organic light-emitting diodes (OLEDs),^[1] organic solar cells,^[2] photodetectors,^[3] organic field-effect transistors (OFETs)^[4], and biotechnologies.^[5] Great efforts have been devoted to the novel structural buildings of conjugated materials, owing to their good solution processability and tunable electronic properties.^[6] Among these materials, the design and synthesis of low-bandgap polymers have drawn greater attention because of their unique properties in optics, electrochemistry as well as better performance in photo devices like OFETs and OLEDs.^[7] Different kinds of low-bandgap polymers have been reported such as polythiophene,^[8] donor-acceptor molecules^[9] and polymers doped with carbon tubes.^[10] With the discovery of the

single-layered graphene,^[11] these graphene nanoribbons^[12] (GNRs) and graphene-like materials^[13] have also caused hotspots in the researches of low-bandgap materials. In the early half of 1997, Roncali reported the five contributions determining the bandgap E_g of π -conjugated systems.^[14]

$$E_g = E^{\delta r} + E^{\theta} + E^{\text{Res}} + E^{\text{Sub}} + E^{\text{Int}}$$

These five factors are the primary instructors for designing low-bandgap polymers. The traditional materials polyphenylenevinylene,^[15] polythiophene^[16] and polyfluorene^[17] are synthesized by the factor $E^{\delta r}$, representing the energy related to the degree of bond length alternation. Donor-acceptor polymers^[18] and some nitrogen heterocyclic compounds^[19] are depended on the E^{Res} , the aromatic resonance energy of the cycle. Other kinds of luminescent polymers with substituted groups^[20] are related to the E^{Sub} , the inductive or mesomeric electronic effects of eventual substitution. However, the factor E^{θ} and E^{Int} , the mean deviation from planarity and the intermolecular and interchain coupling in the solid state, are seldom considered to design and prepare the conjugated molecules.^[21] Inspired by this, we synthesize three different, well-defined structures of polycyclic aromatic hydrocarbons (PAHs): **P1-OX**, **P2-OX** and **P3-OX** to explore the effects of E^{θ} and E^{Int} on the molecular level. These designed PAHs have unique configurations with diversity in planarization: **P1-OX** has a linear conformation, **P2-OX** owns a V-type structure and **P3-OX** shares a zigzag shape. We try to determine the effect of planarization (factor E^{θ}) and the interaction of molecular chains (factor E^{Int}) on the properties involving optics, electrochemistry and, especially the narrow bandgap. Moreover, these low-bandgap polymers are successfully verified by OFET devices, paving the way for screening favorable materials in practical applications.

In detailed works, a series of organic methods^[12e, 12f, 22] were taken to synthesize these PAH precursors: **P1**, **P2** and **P3**, which were created by Diels-Alder reaction between tetraphenylcyclopentadienone derivatives and arynes at yields of more than 80%.^[12b, 12e, 22] And then they were oxidized by ferric chloride/nitromethane system,^[23] leading to the final materials: **P1-OX**, **P2-OX** and **P3-OX**. **Scheme 1** gives the total synthetic routes. The alkyl chains where n-butyls are selected here on the phenyl rings are planned to allow the target polymers good solubility in normal organic solvents. The three cyclization products with different degrees of planarity and conjugated diversity bring intriguing properties. Their structures are well characterized by NMR, matrix-assisted laser desorption ionization time-of-flight mass spectrometry (MALDI-TOF MS), Fourier transform infrared spectrometry (FT-IR), gas chromatography-mass spectrometry (GC-MS), Raman, optics, and electrochemical measurements. The two-dimensional grazing-incidence X-ray diffraction (2D-GIXRD) demonstrates their lamellar layer structures and π - π intermolecular stacking effects.^[24] Gel permeation chromatography (GPC) data show the

H. Chen, H. Zhu, Y. Huang, J. Yang, Prof. W. Wang
 Departme State Key Laboratory of Molecular Engineering of
 Polymers, Department of Macromolecular Science
 Fudan University
 Shanghai 200433, P. R. China
 E-mail: weizhiwang@fudan.edu.cn. Tel: +86 21-65643836

Supporting information for this article is available under
<http://dx.doi.org/10.1002/asia.201701061R2>.

excellent \bar{M}_w range from about 5,000 to 70,000 g/mol for **P1** to **P3**. The solution UV-Vis absorption spectra and photoluminescence (PL) emission spectra give us a clear result of the effect of the molecular conformations, while cyclic voltammetry (CV) tests obtain the further information to prove the optic analysis. At last, the OFET devices are assembled to explore the semiconductor properties of these polymers. These fabricated devices work well at a low working voltage and show the typical p-type transporting behaviors with good charge carrier mobility and on/off ratios. These good performances will guide wild potentials of the OFET applications.

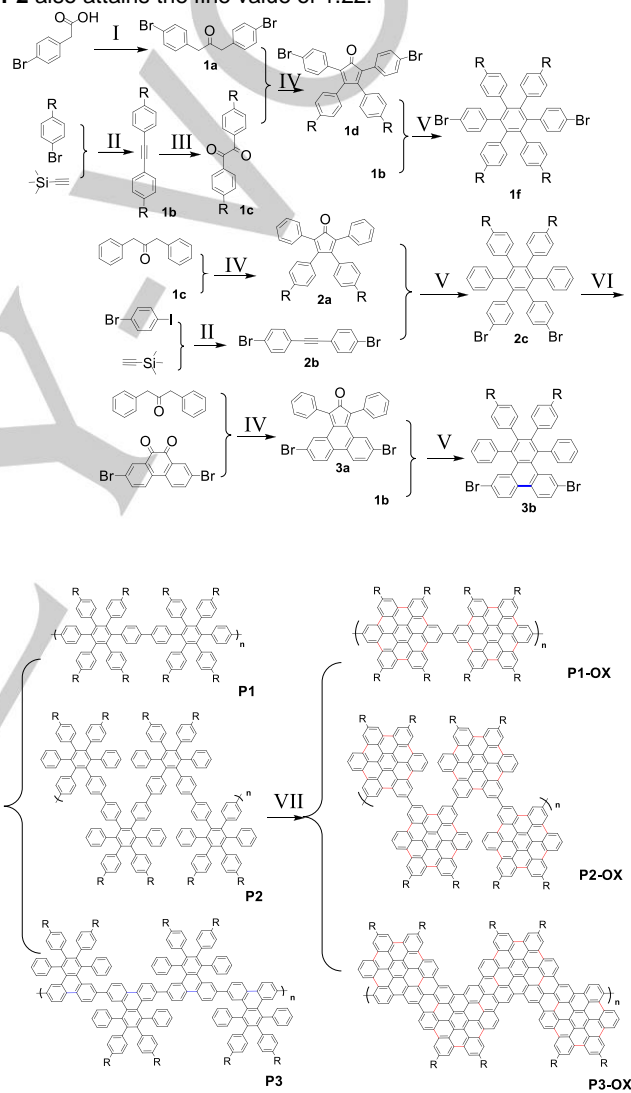
Results and Discussion

Synthesis and structural characterization The synthetic procedures are distinctly illustrated in **Scheme 1**. In these steps, the alkyl chains (n-butyl here) were added to the phenyl rings so as to increase the solubility of the final PAHs in organic solution. When polymerization, for example where **2c** converts into **P2**, the fine solubility of the intermediate product in toluene could obtain a large \bar{M}_w .

The key step of achieving monomers was the Diels-Alder reaction. Based on this reaction, three monomers, **1f**, **2c** and **3b**, were obtained successfully with yields of 81%, 88% and 82%, respectively. The ratio of the two reactants, for instance, **1b** to **1d**, was nearly 1.1:1. The alkyne **1b** was overdosed a bit so that the derivative of tetraphenylcyclopentadienone **1d** could be completely consumed. The purification of **3a** was difficult because of its poor solubility, so we reduced the scale to 1:1 of **1b** to **3a**. The larger hybrid ratio led to a complicated purification. This step was carefully processed in a Schlenk bottle, heated to 280 °C under argon without a solution. When the mixture melted, the reaction temperature should be cooled down to 240 °C. The color of the mixture was dark-claret via the glass bottle. All the monomer reactions were completed between one to two hours, avoiding their carbonization due to such high temperature. After the reaction, the products were isolated by silica gel column chromatography. Generally, most synthesis of hexaphenylbenzene were reacted in solution such as diphenyl ether^[25] at high temperature. But this reaction cannot be treated in solution condition, or the resultant products would have many by-products and a low yield. All the small molecules were characterized by ¹H NMR, ¹³C NMR and FT-IR, while their molecular weights were carefully tested by MALDI-TOF MS and GC-MS. These data are presented in **Figure S13-50** (Supporting Information).

And then the traditional Yamamoto reaction^[26] was adopted to gain the polymers **P1** to **P3** using Ni(COD)₂ as a catalyst in toluene. Traditionally, such polymerization was adopted by the conventional Suzuki-Miyaura coupling.^[27] But the purification of the borate ester monomers was complicated, generally the pure crystal was obtained by recrystallization, which lost some productivity. Compared with Suzuki polymerization, this Yamamoto polymerization was simpler, because the pure monomers were much easier to be gained. Besides, the reaction must be protected by an inert gas like argon owing to the great

oxygen sensitivity of the catalyst. After stirring for five days, the reaction fluid was poured into methanol, and the crude products precipitated. The Soxhlet apparatus was adopted to purify the crude polymers in acetone, refluxed for four days. The GPC with THF as the eluent and the polystyrene as the standard shows the favorable \bar{M}_w of these products **P1** to **P3** to be 9000, 5500 and 69000, respectively. The significant weight-average molecular weights present the successful synthesis of the PAH precursors, especially the relatively huge \bar{M}_w of **P3** whose value reaches 69000. The excellent molecular weights are rare in this polymerization route. Among them, the polydispersity index of **P2** also attains the fine value of 1.22.



Scheme 1. The synthetic routes for PAHs. Reaction conditions: I: DCC, DMAP, CH₂Cl₂ (sol), 25 °C; II: Pd(PPh₃)₄, CuI, DBU, toluene (sol), 50 °C; III: PdCl₂, CuCl₂, DMSO (sol, oxidant), 140 °C; IV: KOH (dissolved by ethanol), ethanol (sol), 85 °C; V: Argon, 240 °C; VI: bipy, Ni(COD)₂, toluene, cyclooctadiene, 85 °C; VII: FeCl₃/CH₃NO₂, 25 °C. More detailed information is given in the text and the supporting information.

The MALDI-TOF MS spectra display the distinct molecular formulas of **P1** to **P3** in **Figure 1** and **S1-S3** (Supporting Information). As described in the pictures, these values 757.1, 644.9 and 642.9 are the repeating unit's molecular weight of **P1**,

For internal use, please do not delete. Submitted_Manuscript

P2 and **P3**, respectively. Each interval between the adjacent molecular weight is almost equal. The value of every repeating unit has a subtle difference because of the isotope effect. These data make it clear that these designed compounds are successfully created. (The polymerization has been proceeded for multiple times for each monomer. Here we exhibit the proper results, so there has some differences in molecular weights.)

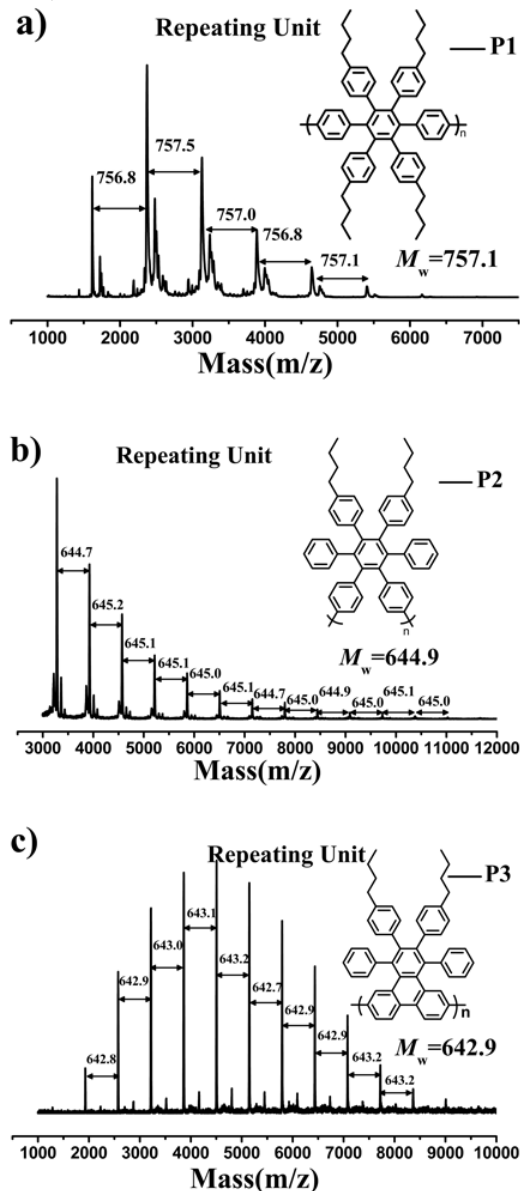


Figure 1. MALDI-TOF MS spectra: (a) **P1**; (b) **P2**; and (c) **P3**. The chemical structures shown in the right side are the schemes of the repeating unit of each compound.

For the last step, a mild intramolecular oxidative dehydrocyclization was adopted to prepare the polymers with the near-planar architecture. The iron (III) chloride/nitromethane system was utilized to oxidize three PAH precursors (**P1**, **P2** and **P3**), as shown in **Scheme 1**. This type of Scholl reaction was usually utilized to synthesize this kind of PAHs on account of its inhibition of the dealkylation and the migration of the alkyl substituents.^[28] After being oxidized for three days kept away from light, the sheet PAH materials were obtained.

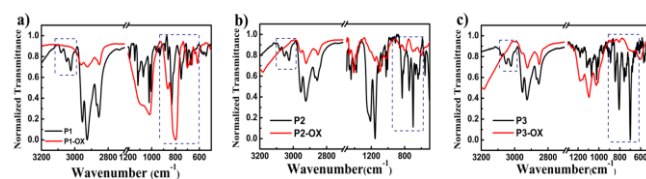


Figure 2. Part of FT-IR spectra within middle infrared regions (3200-2800 cm^{-1} and 1200-600 cm^{-1}): (a) **P1** and **P1-OX**; (b) **P2** and **P2-OX**; and (c) **P3** and **P3-OX**. Transmittance is normalized.

The cyclization process is confirmed by a FT-IR whose results are shown in **Figure 2**. Comparing the FT-IR spectra of the precursors with the ones of the dehydrogenated products, we have a visualized image of the efficiency of dehydrocyclization. As an instance illustrated in **Figure 2b**, these noticeable triad peaks of the aromatic C-H stretching vibrations at 3080, 3050 and 3027 cm^{-1} have obviously disappeared after the cyclization, which verifies the right conversion from **P2** to **P2-OX**. Additionally, these weakened out-of-plane C-H bending vibrations at 825, 750 and 693 cm^{-1} , representing the substituted number and position of phenyl rings, show that there has been a great diversity between **P2** and its cyclization product. Furthermore, the FT-IR spectra in the near-infrared region are shown in **Figure S73-75**. This characteristic broad band at about 4050 cm^{-1} is regarded as an obvious judgement of the existence of free rotating phenyl rings. The disappearance of this peak in the spectra indirectly illustrates the absence of the protons on the phenyl rings. The typical FT-IR data illustrate the transition from precursors to the final PAHs. The ^1H NMR spectra of these precursors and oxidation products are shown in **Figure S4-6** and **S10-12** (Supporting Information). It is pronounced that those peaks ranged from 6 to 8 ppm, the hydrogen on the phenyl rings are broadened after the dehydrocyclization (phenyl ranges are zoomed in). After the dehydrocyclization, the decreased numbers of hydrogen are almost accordance with the theoretical calculations. That means, by the effect of the oxidant (FeCl_3), the C-C bonds are formed within phenyl rings, generating more conjugated phenyl rings, which is a sufficient evidence to demonstrate the oxidation. The nearly consistent spectra of ^{13}C NMR between **P1** and **P1-OX** further identify that the carbon skeletons are not changed after oxidation (**Figure S69** and **70**). There are mainly two types of signals at about 140 ppm and 130 ppm. The peaks at 131 and 126 ppm, representing the sp^2 carbon attached to hydrogen, are broadened due to the loss of the protons after the cyclization. This means most of the carbons are bonded to other ones after the Scholl reaction. Other two ^{13}C NMR spectra of **P2-OX** and **P3-OX** are given in the **Figure S71** and **72**, respectively. Altogether, these distinctive evidences confirm the successful dehydrocyclization.

2D-GIXRD was utilized to study the refined structures of 50-100 nm polymer films in the micro-fields. Generally, conjugated polymers have some orientations of crystallization when having an aggregation, which reflects the interaction of the molecular chains in the solid state, the factor E^{nt} . And this factor of the aggregated structures would highly affect the performance when polymers are used as a semiconductor layer in an OFET device.^[29] The 2D-GIXRD is dynamically fit to the detection of crystal structures of these compounds. Three polymers (**P1-OX** to **P3-OX**) were tested by spin-coating on the Si/SiO₂ substrates

For internal use, please do not delete. Submitted_Manuscript

from a solution of 0.1 weight% (wt%) in chloroform at room temperature. Then these coated films were annealed at 50 °C for about one hour. Mainly, there are two kinds of reflection shown in 2D-GIXRD patterns. The (h00) and the (010) reflection represent the lamellar layer structure and the intermolecular π - π stacking, respectively. (h represents the number 1 or 2)

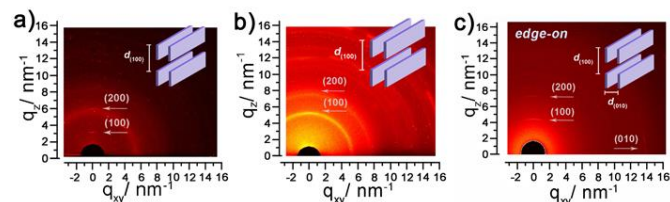


Figure 3. 2D-GIXRD patterns: (a) **P1-OX**; (b) **P2-OX**; and (c) **P3-OX**. The insets in the images are the schemes of the orientation of their aggregation structures. The degree of the 2D-GIXRD is 0.2 degrees.

Figure 3 displays the 2D-GIXRD patterns of the oxidation products which present the edge-on chain conformations. The (100) and (200) planes labelled in **Figure 3a** illustrate that **P1-OX** possesses some crystal orientation in z axis whose d -spacing is 2.42 nm at $q = 2.6 \text{ nm}^{-1}$ (the (100) reflection). The interlamellar space is much broader than the other two ones because of the effect of the extra *n*-butyl chains on its crystallization capacity. These dim diffraction lines mean that the **P1-OX** exhibits the low extent of crystallization because of its low degree of planarity and conjugation. This relatively twisty configuration makes the crystallization ability lowered. The 2D-GIXRD pattern of **P2-OX** also shows the lamellar planes with a prominent bright (100) diffraction facula, shown in **Figure 3b**. The brightness of the middle diffraction is much stronger than that of the marginal parts. The d -spacing of the (100) reflection is 1.23 nm at $q = 5.1 \text{ nm}^{-1}$. The oxidation product **P3-OX**, with a very regular planarity, shares both the lamellar plane with the (100) and (200) diffractions and the intermolecular π - π stacking with the (010) diffraction (in **Figure 3c**), demonstrating the edge-on chain conformation and high crystallinity in a specific orientation. This result also implies that the **P3-OX** maintains the excellent coplanarity backbones comparing with **P1-OX** and **P2-OX**. The d -spacing of the (100) reflection normal to the substrate is 1.19 nm at $q = 5.3 \text{ nm}^{-1}$, and the distance of the π - π stacking parallel to the substrate is 0.45 nm at $q = 14.1 \text{ nm}^{-1}$. These appearances of 2D-GIXRD patterns show the ordered orientations of their aggregation in the film, reflecting intuitively the interaction of molecular chains in the solid state, the factor E^{nt} . These different crystallized orientations would affect the performance in the OFET devices.

Raman spectrometry is an ideal characterization method to research the subtle structures of PAHs due to their similar conformations of GNR. The powder compounds are deposited on a microslide with the laser excitation at 532 nm. The normal graphene sample has two typical peaks: the D band at 1350 cm^{-1} nearby and the G band at about 1580 cm^{-1} , and a G' band also exists at about 2700 cm^{-1} which approximately doubles the number of the D band. **Figure 4** shows the Raman spectra of the three cyclization products: **P1-OX**, **P2-OX** and **P3-OX**, marked in royal, red and olive, respectively. As an example, the Raman pattern of **P3-OX** (in olive line) shows the sharp G band,

representing the aromatic sp^2 carbon symmetric stretching vibrations in-plane, and the D band, representing the structural defect of graphene, locating at 1605 cm^{-1} and 1324 cm^{-1} , respectively. The two bands prove that the fine construction of the PAH. **P3-OX** also shows the specific G' (2D) band, representing the stacking mode (also reflected in the 2D-GIXRD pattern) between the layers of the PAH, located at 2658 cm^{-1} . Another two sets have the same results. More detailed information is given in **Figure S51-53** (Supporting Information).

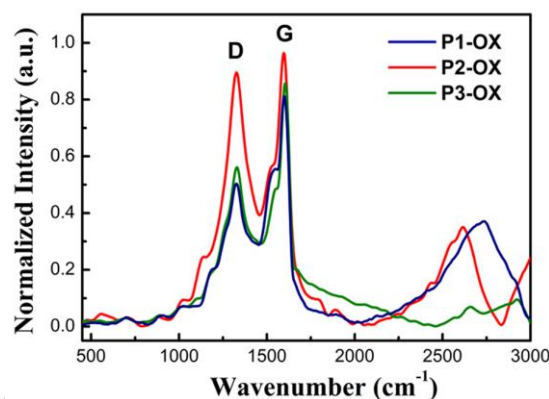


Figure 4. Raman spectra of **P1-OX**, **P2-OX** and **P3-OX** are measured at 532 nm laser excitation at room temperature.

Optical properties The UV-Vis absorption spectra and the PL emission spectra are applied (**Figure 5**) in dilute chloroform solutions (10^{-5} M) to understand the changes in optical properties after dehydrocyclization, and how these subtle changes of planarization influence their color.

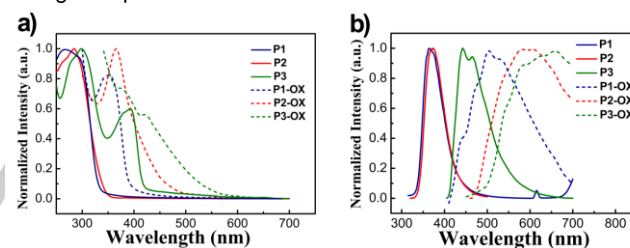


Figure 5. (a) UV-Vis absorption spectra of precursors **P1** to **P3** and their cyclization products **P1-OX** to **P3-OX**; (b) PL emission spectra of precursors **P1** to **P3** and their cyclization products **P1-OX** to **P3-OX**. These vertical ordinates are normalized, and the compounds are dissolved in the dilute chloroform solution (10^{-5} M). **P1**, **P2** and **P3** are identified in solid lines, while **P1-OX**, **P2-OX** and **P3-OX** are outlined in dash lines.

The UV-Vis absorption spectra peaks located at 285, 289 nm are corresponding to **P1** and **P2** (solid lines in royal and red in **Figure 5a**). The two peaks are the phenyl rings π - π^* transition values which are added with the increasing degree of conjugation. Remarkably, **P3** has two peaks lying on 298 and 393 nm (**Figure 5a** with an olive solid line). The peak 298 nm is the π - π^* transition value which redshifts a little. Intriguingly, the chloroform solution of **P3** emits the sky-blue light under the UV lamp at 365 nm (corresponding to 393 nm). The reason is, presumably, **P3** has a higher degree of planarity compared with the other two structures. A special C-C bond between the phenyl rings which is different from **P1** and **P2** is marked with a blue line in **Scheme 1**. The UV-Vis absorption spectra of **P1** and **P2** are only based on the conjugation of flexible benzene rings. These

For internal use, please do not delete. Submitted_Manuscript

benzene rings can rotate freely, so a large planar system is in absence. But **P3** has the planar system with the connection of three phenyl rings. This slightly increased planarization blocks the free rotation of partial phenyl rings, which makes **P3** have another absorption point in the longer wavelength.

All the peaks of the three PAHs: **P1-OX**, **P2-OX** and **P3-OX**, which are located at 352, 366 and 424 nm, respectively (Figure 5a in dash lines) have a clear redshift after the cyclization, indicating that the electron energy level between the first excited state and the ground state becomes narrow. The rigid plane restricts the rotation of phenyl rings, while at the same time the super delocalized π bonds are formed stably by the effect of the oxidation, which increases the degree of the π -electron delocalization and the planarization. These two factors promote the redshift of the UV-Vis absorption spectra simultaneously. This reason also explains the ascending order of the UV-Vis absorption spectra peaks corresponding to the three polymers **P1-OX**, **P2-OX** and **P3-OX**. The three PAHs have different main chain configurations: **P1-OX** has a linear chain, **P2-OX** has the V-type chain and **P3-OX** has the zigzag chain. The former one has an enormous degree of freedom, and even between the repeating units, there is still enough space for the free rotation which would reduce the extent of planarity. This factor results in a relatively small absorption at 352 nm of **P1-OX**. Comparatively, **P2-OX** and **P3-OX** have well-defined structures, especially **P3-OX**. From Scheme 1, we have a clear view that after cyclization, this type of PAH (**P3-OX**) has the most admirable integrity of the arrangements. This structure provides a wide range of space for transmission of the π -electrons due to its favorable degree of planarity so that the maximum absorption peak of **P3-OX** is larger than that of the other two ones. The PL emission spectra are shown in Figure 5b. **P1**, **P2** and **P3** have the peaks at 364, 373 and 443 nm, respectively, while the peaks of **P1-OX**, **P2-OX** and **P3-OX** locate at 502, 589 and 660 nm, respectively. These records, including UV-Vis absorption and PL emission spectra, are wholly listed in Table 1.

Table 1. Optical and electrochemical characteristics of P1, P2, P3, and their dehydrocyclization products.

Compound	$\lambda_{\text{abs}}^{[a]}$ (nm)	$\lambda_{\text{em}}^{[a], [b]}$ (nm)	$E_g^{[c]}$ (eV)	$E_{\text{onset-ox}}^{[d]}$ (V)	$E_{\text{HOMO}}^{[e]}$ (eV)	$E_{\text{LUMO}}^{[f]}$ (eV)
P1	285	364	3.66	1.57	-6.32	-2.66
P1-OX	352	502	2.96	1.38	-6.13	-3.17
P2	289	373	3.64	1.21	-5.96	-2.32
P2-OX	366	589	2.61	1.16	-5.91	-3.30
P3	393	443	2.99	1.14	-5.89	-2.90
P3-OX	424	660	2.44	0.90	-5.65	-3.21

[a] The measurements were tested in a chloroform solution (10^{-5} M). The peak is the maximum absorption position. [b] The emission value is determined by the maximum intensity. [c] The bandgap is calculated from the intersection of the UV-Vis absorption spectra curves and the PL emission spectra curves. ($E_g = 1240/\lambda_{\text{cross}}$). [d] The Eonset-ox is the onset potential for oxidation calculated by CV curves. [e] The HOMO value is calculated by the empirical equation: $E_{\text{HOMO}} = -e(E_{\text{onset-ox}} - 0.0468) - 4.8$ eV. [f] $E_{\text{LUMO}} = E_g + E_{\text{HOMO}}$.

The PL emission spectra has also witnessed the redshift related to these oxidized compounds (**P1-OX** to **P3-OX**) when more phenyl rings are locked. **P1-OX** shifts about 138 nm compared

with 216 nm transferred by **P2-OX** and 217 nm by **P3-OX**. **P1-OX** possesses a relatively flexible geometrical structure, contrasted with **P3-OX** whose planar formation blocks it from turning over. So **P1-OX** has the minimum emission wavelength compared to the maximum wavelength of **P3-OX**.

We have a preliminary conclusion that the higher planarity of the conjugated system guides the lower excitation energy, so the wavelength has an obvious redshift. The free rotation would break this planarization, which leads to the higher energy of the excited molecules. These red-shift phenomena obviously support how the subtle variation among structural details affects the ability of π -electrons transferring in the conjugated system. Furthermore, optical information deeply reflects the right design of what we expected.

Electrochemical properties The CV measurement is carried out to give a full understanding of the relationship between the electronic properties and the optical ones. The three main parameters: the bandgap (E_g), the highest occupied molecular orbital (HOMO) and the lowest unoccupied molecular orbital (LUMO) are consulted to analyze luminescent materials. The CV curves of **P1** to **P3** and their comparison groups **P1-OX** to **P3-OX** are illustrated in Figure S60-65 (Supporting Information), while the three parameters are listed in Table 1.

The optical bandgap is determined by the intersection of UV-Vis absorption curves and PL emission curves (Figure S54-59, Supporting Information). The bandgap of **P1**, **P2** and **P3** is 3.66, 3.64 and 2.99 eV, respectively, corresponding to these values 2.96, 2.61 and 2.44 eV for **P1-OX**, **P2-OX** and **P3-OX**, respectively. The bandgaps of the two groups (**P1** to **P3** and **P1-OX** to **P3-OX**) have the same downtrend due to their various structural configurations. The rotation restriction and the greatest planarity make **P3-OX** have the minimum bandgap 2.44 eV. Meanwhile, the values of E_g also have a downtrend for each group like **P1** and **P1-OX**. The reason is possibly that with the improvement of the conjugation and the planarity, the electronic transition is facilitated and reduces the energy gap. This evidence clearly indicates that the deviation from planarity (E^{θ}) directly affects the bandgap.

On the other hand, the oxidation onsets also exhibit the same downtrend. The corresponding values of **P1** to **P3** are 1.57, 1.21 and 1.14 V while the data of their cyclization compounds share 1.38, 1.16 and 0.90 V, respectively. These numbers reflect the opposite trend testified by the optical tests, which further demonstrate the right effects of the diverse planar system on the electrochemistry. For example, the CV onset of **P1-OX** is 1.38 V while the value of **P3-OX** is 0.90 V. The explanation of this obvious decline may be that by the effect of planarization, the π -electrons delocalize more rapidly and easily so that the electrons have the stronger departure tendency when a voltage is applied. The result makes the oxidation onset potential of **P3-OX** becomes lower than that of **P1-OX**.

In a short conclusion, the divergences of bandgaps and the oxidation onsets are mainly induced by their different planarity. The measured electrochemical results match quite well with the optical values, and are broadly consistent with the molecular incremental planar degree.

For internal use, please do not delete. Submitted_Manuscript

Thermal properties The thermal properties of **P1-OX** to **P3-OX**, tested by the TGA in nitrogen gas, show great thermal stability. The decomposition onset temperatures of **P1-OX** and **P3-OX** are 448.3 °C and 486.3 °C, respectively. These data are illustrated in **Figure S66-68** (Supporting Information).

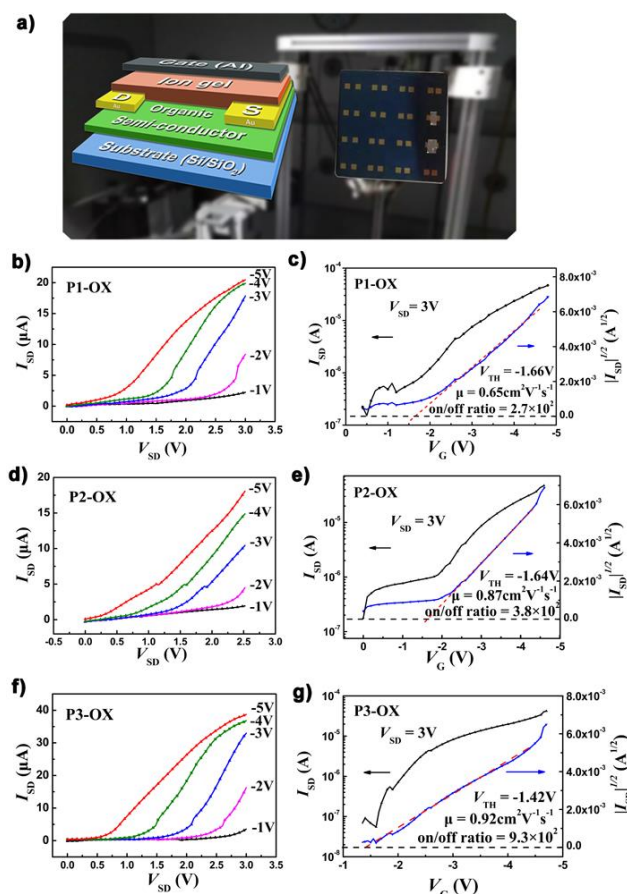


Figure 6. (a) The 3D model shows the geometric structure of the fabricated top-gate OFET; (b), (d) and (f) The output characteristics of the OFET consist of **P1-OX**, **P2-OX** and **P3-OX**, respectively; (c), (e) and (g) The transfer characteristic curves at $V_{SD} = 3$ V of the OFET consist of **P1-OX**, **P2-OX** and **P3-OX**, respectively. V_{SD} is the source-drain voltage.

OFET device performance **Figure 6a** is the image of OFET device made by our group (right), and the 3D model (left) displays concisely the device's structure: a thin film top-gate FET with aluminum as the gate layer and the ionic gel as the dielectric. As a typical example, **Figure 6b** confirms the p-channel FET characteristics as the organic semiconductor layer. The charge carrier mobility (μ) and the threshold voltage (V_{TH}) are the two key parameters which are calculated using the following equation.

$$I_{SD} = \frac{W}{2L} \cdot \mu C_i (V_G - V_{TH})^2$$

The current on/off ratio is calculated from the source-drain current (I_{SD}) versus gate voltage (V_G) illustrated in **Figure 6c, e** and **g**.

In the equation above, the ratio of W (1000 μm), the channel width, to L , the channel length, is equal to 1. C_i is the gate oxide capacitance per unit area whose value is measured as 10 μF

cm^{-2} . **Figure 6b-g** exhibit the characteristics of **P1-OX** to **P3-OX**. The V_{TH} value of **P1-OX** to **P3-OX** is -1.66 V (**Figure 6c**), -1.64 V (**Figure 6e**) and -1.42 V (**Figure 6g**), respectively. These voltages are calculated using the linear relationship between the $|I_{SD}|^{1/2}$ versus the V_G curves. The relatively low threshold voltage -1.42 V of **P3-OX** indicates a low initial working voltage. The μ value of each oxidation product is 0.65, 0.87 and 0.92 $\text{cm}^2 \text{V}^{-1} \text{S}^{-1}$, respectively, while the on/off ratio is 2.7×10^2 for **P1-OX** (**Figure 6c**), 3.8×10^2 for **P2-OX** (**Figure 6e**) and 9.3×10^2 for **P3-OX** (**Figure 6g**). The charge carrier mobility 0.92 $\text{cm}^2 \text{V}^{-1} \text{S}^{-1}$ of **P3-OX** as an example is close to the one of amorphous silicon whose μ is about 1 $\text{cm}^2 \text{V}^{-1} \text{S}^{-1}$. As a semiconductor, this number has a large advantage in practical application at a relatively low working voltage of 3V. As described above, **P3-OX** has the great conjugation and planarization system as well as the fine regularity in the solid state. The two factors make the greatest performance on OFET device simultaneously. Also, the on/off ratio has the certain order among the three PAHs. **P1-OX** has the lowest on/off ratio at about 2.7×10^2 , while **P3-OX** has the highest on/off ratio at about 10^3 . The different order of magnitude is also caused by the varying structure between **P1-OX** and **P3-OX**. The minimal degree of planarity brought by **P1-OX** leads to the limited space for electron transferring, so the sensitivity of on/off ratio becomes relatively lower than that of **P3-OX**.

Conclusions

In summary, to study the effect of planarity E^0 and interaction of the molecular chains in the solid state E^{nt} on the bandgap E_g , three polymers: **P1-OX**, **P2-OX** and **P3-OX**, with different extent of planarity, are synthesized through organic routes. Every compound is characterized in detail by NMR, FT-IR, MS and Raman. MALDI-TOF MS spectra of precursors show the visualized distributions of molecular weights, and GPC data express the more detailed information of M_w : 9000 of **P1**, 5500 of **P2**, and 69000 of **P3**. The 2D-GIXRD data reveal the clear features of the lamellar layer structure and the π - π intermolecular stacking, offering the specific crystal orientation of the three cyclization products with the edge-on chain conformations.

The planarity of phenyl rings dramatically changes the optical and electrochemical behaviors. The PL emission spectra interpret specifically that the emission maximum of the oxidation products has a clear redshift compared with **P1**, **P2** and **P3**. The more planar the conjugated system is, the more obvious the extent of the redshift is. The CV results offer a further proof to demonstrate this alternation. Among them, **P3-OX** has the maximum wavelength of PL emission, 660nm, and the minimum bandgap, 2.44 eV, owing to its greatest extent of planarity and conjugation.

In the end, the OFET devices fabricated with final conjugated products as the semiconductor layer possess good results. The admirable top-gated devices gain better performance when the planarity is rising. The best charge carrier mobility 0.92 $\text{cm}^2 \text{V}^{-1}$

For internal use, please do not delete. Submitted_Manuscript

S^{-1} of **P3-OX**, which is close to $1 \text{ cm}^2 \text{ V}^{-1} \text{ S}^{-1}$, exhibits a vast prospect in the practical OFET application.

Experimental Section

Materials

All reagents and chemicals were obtained from reagent companies listed below: Sigma-Aldrich, ACROS Organics, J&K, TCI and Sinopharm Chemical Reagent Company. Solvents were purified by anhydrous treatments.

Instrument methods

^1H NMR and ^{13}C NMR spectra were recorded in CD_2Cl_2 and CDCl_3 on Bruker AVANCE III HD 400 MHz FT-NMR spectrometer with tetramethylsilane (TMS) as the internal standard. Molecular weights were measured on an AB SCIEX 5800 MALDI-TOF Mass Spectrometer and PE680-ST8 GC-MS. FT-IR spectra were tested on Nicolet 6700, Thermofisher, using the transmittance method. Raman spectra were performed on the XploRA (HORIBA JobinYvon) spectrometer at 532 nm laser. UV-Vis absorption spectra were analyzed in a solution of CHCl_3 (10^{-5} M) by a Perkin-Elmer Lambda 750 UV-Visible spectrophotometer. PL informations were collected in the chloroform solution (10^{-5} M) by the Fluorescence Spectrometers (Photo Technology International, Inc., QM40). GPC measurement was tested on a spectrometer of Agilent/Wyatt 1260 the polystyrene as the calibration. The 2D-GIXRD data were obtained at beamline BL14B1 of the Shanghai Synchrotron Radiation Facility using X-ray with a wavelength of 1.2398 Å and a grazing-incidence angle of 0.2° . The samples (0.1 wt% chloroform solution) were drop-coated on the Si/SiO_2 substrates. CV method was tested on the CHI 800D electrochemical workstation with a three-electrode cell at a scan rate of 40 mV S^{-1} . An acetonitrile solution of tetrabutylammonium hexafluorophosphate (0.1 M) was prepared as the electrolyte, with ferrocene as an internal standard substance (0.0468 V). Before every test, the solution system must be bubbled by argon at least five minutes in order to expel oxygen. A glass-carbon electrode (the working electrode), a platinum wire (the counter electrode), and an Ag/AgNO_3 electrode (the reference electrode) constituted the three-electrode system together. Thermogravimetric analysis (TGA) was tested by a Thermo Gravimetric Analyzer, Mettler Toledo, with a heating rate of $20 \text{ }^\circ\text{C min}^{-1}$, nitrogen flowed.

Synthesis

Compound 1a: A solution of dicyclohexylcarbodiimide (DCC, 4.8 g, 23.3 mmol) and 4-(dimethylamino)pyridine (DMAP, 0.60 g, 4.6 mmol) in CH_2Cl_2 (100 mL) was stirred without heating under inert gas protection and then added dropwise with a solution of 2-(4-bromophenyl) acetic acid (5.2 g, 24.0 mmol) in CH_2Cl_2 (50 mL). The mixture was stirred at room temperature for 20 hours and then filtered. The solution was removed by reduced pressure, and the product was isolated by flash column chromatography using increasing amounts of ethyl acetate in petroleum ether as eluent. The compound was purified by recrystallization from methanol/hexane. ^1H NMR (400 MHz, CDCl_3 , Me_4Si) δ =7.45 (d, J = 8.4 Hz, 4H), 7.01 (d, J = 8.4 Hz, 4H), 3.68 (s, 4H); ^{13}C NMR (100 MHz, CDCl_3 , Me_4Si) δ =204.28, 132.67, 131.86, 131.24, 121.27, 48.48. FT-IR (cm^{-1}): 2883, 1901, 1716, 1590, 1485, 1411, 1338, 1103, 1055, 1008, 831, 795, 768, 732, 669; GC-MS: m/z 368.

Compound 1b: A 250 mL round bottle flask with a magnetic stirrer was purged with argon and charged with $\text{Pd}(\text{PPh}_3)_4$ (700 mg, 2 mol%), CuI (571 mg, 10 mol%). Dry toluene (100 mL) sparged with argon was added by syringe. Then 1-bromo-4-butylbenzene (6.39 g, 32 mmol) and ethynyltrimethylsilane (1.47 g, 15 mmol) were added in such mixture by syringe. Argon sparged 1,8-diazabicyclo[5.4.0]undec-7-ene (DBU, 27 mL, 180 mmol) and deionized water (0.2 mL, 40 mol%) were also added by syringe under stirring. The reaction was heated to $50 \text{ }^\circ\text{C}$ for 20 hours under the argon. After that, the mixture was extracted with ethyl ether (30 mL) and distilled water (60 mL). The organic layer was washed with 10% hydrochloric acid ($2 \times 70 \text{ mL}$), brine ($2 \times 40 \text{ mL}$), and dried over anhydrous sodium sulphate overnight. The filtered crude product was purified by silica gel column chromatography with pure hexane as eluent. The product **1b** was isolated as colorless crystals at yield 78%. ^1H NMR (400 MHz, CD_2Cl_2 , Me_4Si) δ =7.42 (d, J = 8.4 Hz, 4H), 7.18 (d, J = 8.4 Hz, 4H), 2.62 (t, J = 7.8 Hz, 4H), 1.60 (m, J = 7.6 Hz, 4H), 1.36 (m, J = 7.6 Hz, 4H) 0.93 (t, J = 7.2 Hz, 6H); ^{13}C NMR (100 MHz, CDCl_3 , Me_4Si) δ =143.35, 131.64, 128.62, 120.82, 89.1, 35.78, 33.61, 22.51, 14.13; FT-IR (cm^{-1}): 3036, 1914, 1662, 1513, 1458, 1370, 1115, 1014, 928, 829, 776, 735; GC-MS: m/z 290.

Compound 1c: A mixture of 1,2-bis(4-butylphenyl)ethyne (**1b**) (2.9 g, 10 mmol), PdCl_2 (88.5 mg, 0.5 mmol) and CuCl_2 (134 mg, 1 mmol) in 100 mL DMSO was stirred at $140 \text{ }^\circ\text{C}$ for 10 hours. After cooling to room temperature, the mixture was extracted with ethyl acetate ($2 \times 70 \text{ mL}$). The organic layers were then washed with 10% hydrochloric acid ($2 \times 60 \text{ mL}$). The supernatant was collected, dried with anhydrous sodium sulphate and concentrated. The crude product was purified by silica gel column chromatography. The isolated yield of compound **1c** was 82%. ^1H NMR (400 MHz, CDCl_3 , Me_4Si) δ 7.88 (d, J = 8.4 Hz, 4H), 7.30 (d, J = 8.4 Hz, 4H), 2.68 (t, J = 7.8 Hz, 4H), 1.62 (m, J = 7.8 Hz, 4H), 1.35 (m, J = 7.8 Hz, 4H), 0.93 (t, J = 7.4 Hz, 6H); ^{13}C NMR (100 MHz, CDCl_3 , Me_4Si) δ =194.55, 150.96, 130.89, 130.07, 129.09, 35.92, 33.13, 22.30, 13.88; FT-IR (cm^{-1}): 3027, 2929, 2863, 1928, 1676, 1602, 1460, 1318, 1216, 1172, 885, 842, 742, 611; GC-MS: m/z 322.

Compound 1d: A 500 mL round bottle with a magnetic stirrer was charged with **1a** (5.0 g, 15.5 mmol) and **1c** (6.90 g, 18.6 mmol). And then the mixture was diluted with absolute ethanol (120 mL). The reaction mixture was heated to $60 \text{ }^\circ\text{C}$, and then a 15 mL solution of 1.06 g KOH (18.8 mmol) in alcohol was added dropwise. The reaction was stirred vigorously at $85 \text{ }^\circ\text{C}$ for 2.5 hours. And then stop the reaction, the wine-red liquid was obtained. The mixture was extracted with chloroform and distilled water (60 mL, each). Then the organic layer was washed with 10% hydrochloric acid ($3 \times 30 \text{ mL}$), and then brine ($1 \times 50 \text{ mL}$), dried with anhydrous magnesium sulphate over 1h. The crude product was purified by silica gel column chromatography with hexane/dichloromethane = 8/2 as eluent. A bright wine-red solid was collected at an isolated yield 65%. ^1H NMR (400 MHz, CD_2Cl_2 , Me_4Si) δ =7.36 (d, J = 8.4 Hz, 4H), 7.11 (d, J = 8.8 Hz, 4H), 6.98 (d, J = 8.4 Hz, 4H), 6.78 (d, J = 8.4 Hz, 4H), 2.40 (t, J = 7.6 Hz, 4H), 1.41 (m, J = 7.2 Hz, 4H), 1.15 (m, J = 8.0 Hz, 4H), 0.85(t, J = 7.6 Hz, 6H); FT-IR (cm^{-1}): 3033, 2926, 1908, 1706, 1606, 1485, 1340, 1070, 1009, 819, 762; MS (MALDI-TOF): m/z 655.3130.

General method of **1f**: Compound **1d** (2.5 g, 3.8 mmol) and **1b** (1.11 g, 3.8 mmol) were mixed in a 25 mL Schlenk bottle without a stirrer. This system was heated to $280 \text{ }^\circ\text{C}$ under argon protection until the mixture melted, and then the temperature was cooled down to $240 \text{ }^\circ\text{C}$, maintaining for one hour. After cooling down the reaction, dichloromethane was added into this container. The raw product was isolated by silica gel column chromatography. The solvent was removed by vacuum, and a white crystal was gained at yield 81%. ^1H NMR (400 MHz, CD_2Cl_2 , Me_4Si) δ =6.96 (d, J = 8.4 Hz, 4H), 6.72-6.69 (m, 20H), 2.39

For internal use, please do not delete. Submitted_Manuscript

(t, $J = 7.4$ Hz, 8H), 1.40 (m, $J = 7.4$ Hz, 8H), 1.13 (m, $J = 7.4$ Hz, 8H), 0.84 (t, $J = 7.2$ Hz, 12H); ^{13}C NMR (100 MHz, CDCl_3 , Me_4Si) $\delta=140.36$, 139.96, 139.58, 139.32, 137.50, 133.07, 131.12, 129.62, 126.84, 119.18, 35.00, 33.28, 21.77, 13.95; FT-IR (cm^{-1}): 3019, 2925, 2857, 1902, 1633, 1514, 1489, 1384, 1069, 1010, 859, 832, 755; MS (MALDI-TOF): m/z 916.5406.

Compound **3a**: 5.34 g (14.6 mmol) of 2,7-dibromophenanthrene-9,10-dione and 1,3-diphenylpropan-2-one (3.7 g 17.6 mmol) were added to 40 mL methanol under stirring. This mixture was refluxed, and then a 50 mL solution of 0.3 M KOH (15.0 mmol) in methanol was added dropwise. Then the reaction system vigorously stirred at 80 °C. After stirring for 2.5 h, the reaction was stopped and filtered to get the product. A dark green solid was obtained and washed with methanol. The substance was dried under reduced pressure to obtain 4.5 g of **3a** at 54% yield without other purification. ^1H NMR (400 MHz, CD_2Cl_2 , Me_4Si) $\delta=6.96$ (d, $J = 8.4$ Hz, 4H), 6.72-6.69 (m, 20H), 2.39 (t, $J = 7.4$ Hz, 8H), 1.40 (m, $J = 7.4$ Hz, 8H), 1.13 (m, $J = 7.4$ Hz, 8H), 0.84 (t, $J = 7.2$ Hz, 12H); ^{13}C NMR (100 MHz, CDCl_3 , Me_4Si) $\delta=140.36$, 139.96, 139.58, 139.32, 137.50, 133.07, 131.12, 129.62, 126.84, 119.18, 35.00, 33.28, 21.77, 13.95; FT-IR (cm^{-1}): 3019, 2925, 2857, 1902, 1633, 1514, 1489, 1384, 1069, 1010, 859, 832, 755; MS (MALDI-TOF): m/z 916.5406.

General polymerization of **P1**: 420 mg **1f** (0.46 mmol), 200 mg $\text{Ni}(\text{COD})_2$ (0.7 mmol, COD = cyclooctadiene) and 450 mg 2,2'-bipyridine (2.8 mmol) were mixed in a 50 mL Schlenk bottle under dry argon atmosphere with a magnetic stirrer. 30 mL dried toluene and 5 mL cyclooctadiene were added into this system by syringe. The reaction must proceed without the presence of water and oxygen. With strong stirring, the mixture was heated to 80 °C for five days, and then the crude product was obtained by participation from methanol. The crude product was reflux in acetone using Soxhlet extraction equipment for four days. Then the clean polymers were gotten. ^1H NMR, MS and GPC data were given in **Figure S1-9** (Supporting Information).

General synthesis of P1-OX: 20 mg **P1** was put into a 10 mL glass bottle, and then dissolved by argon-sparged dichloromethane. A saturated ferric chloride solution dissolved by nitromethane was added in the bottle. After stirring three days, the reaction was washed with 10% hydrochloric acid (2x30 mL) and a large amount of deionized water. The solution was removed by vacuum at 100 °C, and then the lamellar product was observed. ^1H NMR data are given in **Figure S10-12**, and ^{13}C NMR informations are in **Figure S69-72** (Supporting Information).

Fabrication of the OFET devices

The p-doped SiO_2 (300 nm)/Si wafers (square shape) which are commercially available were washed with $\text{H}_2\text{O}_2/\text{H}_2\text{SO}_4$, deionized water, acetone and methanol. The polymers in CHCl_3 solution (about 1 mg mL^{-1}) were spin-coated on these non-polluted silicon surfaces at the rotating speed of 4000 r min^{-1} . To evaporate the surplus solvent after spinning, the obtained thin films were placed in a vacuum drying chamber over 1h at 50 °C. A 50 nm thick gold source and drain electrode was vapor-deposited on the polymer thin film. A kind of ionic solution was used as the top gate dielectrics, mixed by water, prepared ionic gel and ionic liquid with a ratio of 20:9.5:0.5, where the ionic gel was the triblock copolymer mixture of poly(styrene block-methyl methacrylate-block styrene) (PS-PMMA-PS; $M_{\text{PS}} = 5.5 \text{ kg mol}^{-1}$, $M_{\text{PMMA}} = 13.7 \text{ kg mol}^{-1}$, $M_{\text{W}} = 22.3 \text{ kg mol}^{-1}$), and the ionic liquid was the ethyl propionate solution mixed with 1-ethyl-3-methylimidazolium bis(trifluoromethylsulfonyl)imide. Then the transistor channels were concealed by a foil of aluminum (0.02 mm) to become the top-gate electrode. In the end, a thin gold wire, as a reference electrode, was inserted into the gel films to integrate the device.

Acknowledgements

This work was financially supported by the National Natural Science Foundation of China (21274027 and 20974022) and the Innovation Program of Shanghai Municipal Education Commission (15ZZ002).

The authors thank beamline BL14B1 (Shanghai Synchrotron Radiation Facility) for providing the beam time and helps during experiments.

Keywords: low bandgap materials • conjugated polymers • polycyclic aromatic hydrocarbons • luminescent materials • organic field-effect transistors

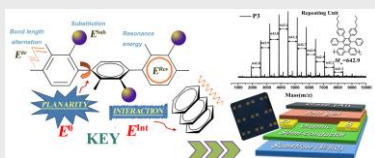
- [1] a) S. Reineke, F. Lindner, G. Schwartz, N. Seidler, K. Walzer, B. Lüssem, K. Leo, *Nature* **2009**, *459*, 234-238; b) J. Wu, M. Agrawal, H. A. Becerril, Z. Bao, Z. Liu, Y. Chen, P. Peumans, *ACS Nano* **2009**, *4*, 43-48.
- [2] a) S. Günes, H. Neugebauer, N. S. Sariciftci, *Chem. Rev.* **2007**, *107*, 1324-1338; b) W. Ma, C. Yang, X. Gong, K. Lee, A. J. Heeger, *Adv. Funct. Mater.* **2005**, *15*, 1617-1622; c) B. C. Thompson, J. M. J. Fréchet *Angew. Chem. Int. Ed.* **2008**, *47*, 58-77.
- [3] a) K. J. Baeg, M. Binda, D. Natali, M. Caironi, Y. Y. Noh, *Adv. Mater.* **2013**, *25*, 4267-4295; b) P. Peumans, A. Yakimov, S. R. Forrest, *J. Appl. Phys.* **2003**, *93*, 3693-3723; c) W. Huang, E. Smarsly, J. Han, M. Bender, K. Seehafer, I. Wacker, R. R. Schroeder, U. H. F. Bunz, *ACS Appl. Mater. Interfaces* **2017**, *9*, 3068-3074.
- [4] a) S. Liu, W. M. Wang, A. L. Briseno, S. C. B. Mannsfeld, Z. Bao, *Adv. Mater.* **2009**, *21*, 1217-1232; b) A. R. Murphy, J. M. J. Fréchet, *Chem. Rev.* **2007**, *107*, 1066-1096; c) Z. Zhao, Z. Yin, H. Chen, L. Zheng, C. Zhu, L. Zhang, S. Tan, H. Wang, Y. Guo, Q. Tang, Y. Liu, *Adv. Mater.* **2017**, *29*, 1602410
- [5] M. E. Davis, Z. G. Chen, D. M. Shin, *Nat. Rev. Drug Discovery* **2008**, *7*, 771-782.
- [6] a) J. Mei, Y. Diao, A. L. Appleton, L. Fang, Z. Bao, *J. Am. Chem. Soc.* **2013**, *135*, 6724-6746; b) C. Wang, H. Dong, W. Hu, Y. Liu, D. Zhu, *Chem. Rev.* **2011**, *112*, 2208-2267.
- [7] a) J. Chen, J. Zhang, Y. Zou, W. Xu, D. Zhu, *J. Mater. Chem. A* **2017**, *5*, 9891-9896; b) A. J. Kronemeijer, E. Gili, M. Shahid, J. Rivnay, A. Salleo, M. Heeney, H. Sirringhaus, *Adv. Mater.* **2012**, *24*, 1558-1565; c) L. Ying, F. Huang, G. C. Bazan, *Nat. Commun.* **2017**, *8*, 14047; d) A. Candini, L. Martini, Z. Chen, N. Mishra, D. Convertino, C. Coletti, A. Narita, X. Feng, K. Müllen, M. Affronte, *J. Phys. Chem. C* **2017**, *121*, 10620-10625.
- [8] a) R. Joseph Kline, M. D. McGehee, M. F. Toney, *Nat. Mater.* **2006**, *5*, 222-228; b) R. Joseph Kline, M. D. McGehee, E. N. Kadnikova, J. Liu, J. M. J. Fréchet, *Adv. Mater.* **2003**, *15*, 1519-1522; c) J. Roncali, *Chem. Rev.* **1992**, *92*, 711-738.
- [9] a) R. Stalder, J. Mei, K. R. Graham, L. A. Estrada, J. R. Reynolds, *Chem. Mater.* **2014**, *26*, 664-678; b) A. Facchetti, *Mater. Today* **2013**, *16*, 123-132; c) T. Lei, J. Y. Wang, J. Pei, *Acc. Chem. Res.* **2014**, *47*, 1117-1126.
- [10] D. M. Guldi, G. Rahman, F. Zerbetto, M. Prato, *Acc. Chem. Res.* **2005**, *38*, 871-878.
- [11] a) K. S. Novoselov, A. K. Geim, S. V. Morozov, D. Jiang, Y. Zhang, S. V. Dubonos, I. V. Grigorieva, A. A. Firsov, *Science* **2004**, *306*, 666-669; b) J. Wu, W. Pisula, K. Müllen, *Chem. Rev.* **2007**, *107*, 718-747.
- [12] a) T. H. Vo, M. Shekhirev, D. A. Kunkel, M. D. Morton, E. Berglund, L. Kong, P. M. Wilson, P. A. Dowben, A. Enders, A. Sinitskii, *Nat. Commun.* **2014**, *5*, 3189; b) A. Narita, X.-Y. Wang, X. Feng, K. Müllen, *Chem. Soc. Rev.* **2015**, *44*, 6616-6643; c) A. Narita, I. A. Verzhbitskiy,

For internal use, please do not delete. Submitted_Manuscript

- W. Frederickx, K. S. Mali, S. A. Jensen, M. R. Hansen, M. Bonn, S. De Feyter, C. Casiraghi, X. Feng, K. Müllen, *ACS Nano* **2014**, *8*, 11622-11630; d) Z. Chen, H. I. Wang, J. Teyssandier, K. S. Mali, T. Dumslaff, I. Ivanov, W. Zhang, P. Ruffieux, R. Fasel, H. J. Räder, D. Turchinovich, S. De Feyter, X. Feng, M. Kläui, A. Narita, M. Bonn, K. Müllen, *J. Am. Chem. Soc.* **2017**, *139*, 3635-3638; e) T. H. Vo, M. Shekhirev, D. A. Kunkel, F. Orange, M. J. F. Guinel, A. Enders, A. Sinitskii, *Chem. Commun.* **2014**, *50*, 4172-4174; f) M. Shekhirev, A. Sinitskii, *Chem. Carbon Nanostructures* **2017**, 194-225; g) J. D. Teeter, P. S. Costa, M. Mehdi Pour, D. P. Miller, E. Zurek, A. Enders, A. Sinitskii, *Chem. Commun.* **2017**, *53*, 8463-8466.
- [13] a) A. Narita, X. Feng, K. Müllen, *Chem. Rec.* **2015**, *15*, 295-309; b) X. Y. Wang, T. Dienel, M. Di Giovannantonio, G. B. Barin, N. Khariche, O. Deniz, J. I. Urgel, R. Widmer, S. Stolz, L. H. De Lima, M. Muntwiler, M. Tommasini, V. Meunier, P. Ruffieux, X. Feng, R. Fasel, K. Müllen, A. Narita, *J. Am. Chem. Soc.* **2017**, *139*, 4671-4674; c) Z. Xu, X. Zhuang, C. Yang, J. Cao, Z. Yao, Y. Tang, J. Jiang, D. Wu, X. Feng, *Adv. Mater.* **2016**, *28*, 1981-1987.
- [14] J. Roncali, *Chem. Rev.* **1997**, *97*, 173-205.
- [15] J. H. Burroughes, D. D. C. Bradley, A. R. Brown, R. N. Marks, K. Mackay, R. H. Friend, P. L. Burns, A. B. Holmes, *Nature* **1990**, *347*, 539-541.
- [16] N. Zhao, N. Ai, M. Cai, X. Wang, J. Pei, X. Wan, *Polym. Chem.* **2016**, *7*, 235-243.
- [17] a) A. Yokoyama, H. Suzuki, Y. Kubota, K. Ohuchi, H. Higashimura, T. Yokozawa, *J. Am. Chem. Soc.* **2007**, *129*, 7236-7237; b) D. Veldman, O. İpek, S. C. J. Meskers, J. Sweelssen, M. M. Koetse, S. C. Veenstra, J. M. Kroon, S. S. van Bavel, J. Loos, R. A. J. Janssen, *J. Am. Chem. Soc.* **2008**, *130*, 7721-7735.
- [18] P. M. Beaujuge, C. M. Amb, J. R. Reynolds, *Acc. Chem. Res.* **2010**, *43*, 1396-1407.
- [19] U. H. F. Bunz, *Acc. Chem. Res.* **2015**, *48*, 1676-1686.
- [20] a) J.-H. Dou, Y.-Q. Zheng, T. Lei, S.-D. Zhang, Z. Wang, W.-B. Zhang, J.-Y. Wang, J. Pei, *Adv. Funct. Mater.* **2014**, *24*, 6270-6278; b) J. Mei, Z. Bao, *Chem. Mater.* **2014**, *26*, 604-615.
- [21] a) J. Li, A. Terec, Y. Wang, H. Joshi, Y. Lu, H. Sun, M. C. Stuparu, *J. Am. Chem. Soc.* **2017**, *139*, 3089-3094; b) V. Rajeshkumar, M. Courté, D. Fichou, M. C. Stuparu, *Eur. J. Org. Chem.* **2016**, *36*, 6010-6014.
- [22] a) E. Gagnon, S. D. Halperin, V. Métivaud, K. E. Maly, J. D. Wuest, *J. Org. Chem.* **2010**, *75*, 399-406; b) M. J. Mio, L. C. Kopel, J. B. Braun, T. L. Gadzikwa, K. L. Hull, R. G. Brisbois, C. J. Markworth, P. A. Grieco, *Org. Lett.* **2002**, *4*, 3199-3202; c) M. J. E. Resendiz, M. A. Garcia-Garibay, *Org. Lett.* **2005**, *7*, 371-374.
- [23] a) K. Wunderlich, A. Göelzhäuser, M. Klapper, K. Müllen, in *Polymer Precursor-Derived Carbon, Vol. 1173* (Eds.: A. K. Naskar, W. P. Hoffman), **2014**, pp. 1-16; b) M. El Gemayel, A. Narita, L. F. Döessel, R. S. Sundaram, A. Kiersnowski, W. Pisula, M. R. Hansen, A. C. Ferrari, E. Orgiu, X. Feng, K. Müllen, P. Samori, *Nanoscale* **2014**, *6*, 6301-6314.
- [24] a) H. Yang, S. W. LeFevre, C. Y. Ryu, Z. Bao, *Appl. Phys. Lett.* **2007**, *90*, 172116; b) W. Liu, A. Tang, J. Chen, Y. Wu, C. Zhan, J. Yao, *ACS Appl. Mater. Interfaces* **2014**, *6*, 22496-22505; c) Y. Qu, Q. Su, S. Li, G. Lu, X. Zhou, J. Zhang, Z. Chen, X. Yang, *ACS Macro Lett.* **2012**, *1*, 1274-1278.
- [25] Y. Kikuzawa, T. Mori, H. Takeuchi, *Org. Lett.* **2007**, *9*, 4817-4820.
- [26] a) T. Kanbara, N. Saito, T. Yamamoto, K. Kubota, *Macromolecules* **1991**, *24*, 5883-5885; b) T. Yamamoto, A. Morita, Y. Miyazaki, T. Maruyama, H. Wakayama, Z. Zhou, Y. Nakamura, T. Kanbara, S. Sasaki, K. Kubota, *Macromolecules* **1992**, *25*, 1214-1223; c) J. Schmidt M. Werner, A. Thomas, *Macromolecules* **2009**, *42*, 4426-4429.
- [27] L. Döessel, L. Gherghel, X. Feng, K. Müllen, *Angew. Chem. Int. Ed.* **2011**, *50*, 2540-2543.
- [28] a) P. Rempala, J. Kroulík, B. T. King, *J. Am. Chem. Soc.* **2004**, *126*, 15002-15003; b) C. D. Simpson, G. Mattersteig, K. Martin, L. Gherghel, R. E. Bauer, H. J. Räder, K. Müllen, *J. Am. Chem. Soc.* **2004**, *126*, 3139-3147.
- [29] a) G. Li, Y. Yao, H. Yang, V. Shrotriya, G. Yang, Y. Yang, *Adv. Funct. Mater.* **2007**, *17*, 1636-1644; b) Y. Kim, S. Cook, S. M. Tuladhar, S. A. Choulis, J. Nelson, J. R. Durrant, D. D. C. Bradley, M. Giles, I. McCulloch, C. S. Ha, M. Ree, *Nat. Mater.* **2006**, *5*, 197-203.

Entry for the Table of Contents (Please choose one layout)

FULL PAPER



Hua Chen, Haoyun Zhu, Yuli Huang,
Junwei Yang, and Weizhi Wang*

Page No. – Page No.

Title

Most of the conjugated polymers are prepared based on the factors E^{r} , E^{Res} and E^{Sub} . This paper proposed a brand new method, focusing on another two features, E^{H} and E^{int} . Three polymers with various configurations are designed and their molecular weights are well characterized. These compounds, furthermore, are applied successfully to assemble the OFET devices, providing a new alternative for the future design of electronic devices.